Energy & Environmental Science

Accepted Manuscript

ROYAL SOCIETY OF CHEMISTRY

www.rsc.org/ees

TOC for

Mechanism Investigation and Suppression of Self-discharge in Active Electrolyte Enhanced Supercapacitor

Libin Chen, Hua Bai,* Zhifeng Huang, and Lei Li*

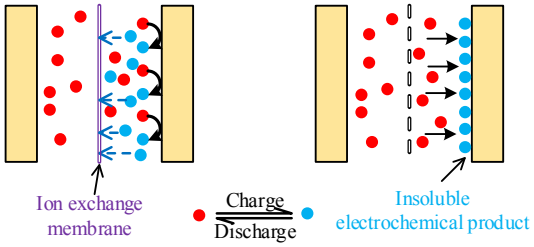

The mechanism of self-discharge (SDC) in active electrolyte enhanced supercapacitor was investigated, and two strategies were devised to suppress the SDC process.

Broader Context

Active electrolyte enhanced supercapacitors (AEESCs) have distinguished themselves as promising devices for electric energy storage due to their high specific capacitance and easy fabrication process. In AEESCs the redox active species, which provide large pseudocapacitance, are dissolved in electrolyte rather than deposited on the electrodes. However, the effects of active electrolyte on the self-discharging (SDC) process of AEESCs have long been neglected. The rate of SDC is the index of the energy retention of a power storage device, and supercapacitors with fast SDC process are of little practical use due to the quick loss of stored energy. In this paper, the SDC process of AEESC was investigated systematically. We found that the migration of active electrolyte between two electrodes of the device strongly accelerated the SDC process. In order to suppress the fast SDC of AEESC, two strategies were devised to stop the migration of active electrolyte. We demonstrated that by using ion exchange membrane as separator, or $CuSO_4$ as active electrolyte, the fast SDC process can be successfully suppressed. These results will shed light on the future design of AEESCs with high capacitance and superior energy retention.

Journal Name

RSCPublishing

ARTICLE

Mechanism Investigation and Suppression of Self-discharge in Active Electrolyte Enhanced Supercapacitor†

Cite this: DOI: 10.1039/x0xx00000x

Libin Chen, Hua Bai,* Zhifeng Huang, and Lei Li*

Received 00th January 2012,
Accepted 00th January 2012

DOI: 10.1039/x0xx00000x

www.rsc.org/

The self-discharge (SDC) process of active electrolyte enhanced supercapacitor (AEESC) was investigated systematically. The AEESC with hydroquinone as active electrolyte showed higher specific capacitance but much faster SDC compared with electronic double layer supercapacitor. The electrode process of the above AEESC was studied, and the mechanism of the SDC process was investigated quantitatively. The migration of active electrolyte between two electrodes of the device was found to be the primary reason for the fast SDC. Two strategies were designed to suppress the migration of active electrolyte. Following these strategies, two new AEESCs were fabricated, with Nafion® membrane as separator, or with $CuSO_4$ as active electrolyte, respectively. The two AEESCs showed both high specific capacitance and long SDC time, demonstrating that the problem of poor energy retention of AEESC was successfully solved.

Introduction

Recent years have witnessed the rapid development of electrochemical supercapacitors.[1–3] Compared with batteries, which store energy throughout the bulk of the electrode material, supercapacitors store charges on the surface of their electrodes (with electric double layer, EDL), thus are able to provide much higher power density (10^3 ~ 10^5 W kg^{-1}).[4] Also supercapacitors have longer cycle life than batteries. These properties make supercapacitors suitable power sources for the applications which demand high charging/discharging current, such as in electric vehicles. Supercapacitors based on EDL (EDLSCs) suffer from low energy density (< 10 Wh kg^{-1}), thus considerable efforts have been devoted to increase their energy density without sacrificing their power density. The energy density of a supercapacitor is decided by both the specific capacitance and the operation voltage, but for EDLSCs based on carbon materials with aqueous electrolyte, the operation voltage is limited to ~ 1 V by the electrochemical window of water, thus the most works are focused on how to increase the specific capacitance. An efficient way to improve the specific capacitance is to incorporate redox active materials into the capacitors, which can store additional energy by electrochemical reaction.[5–8] The redox active materials, such as metal oxide/hydroxides[5] and conducting polymers,[7] are usually coated onto inert carbon electrodes to provide additional capacitance (pseudocapacitance) in a battery-like manner. The asymmetric device structure after incorporation of redox active materials can also increase the operation voltage of the device. With these redox active materials, the specific capacitances of electrode were promoted to over 1000 F g^{-1},[9,10] with corresponding an energy density of > 50 Wh kg^{-1} and power density of ~ 10^3 W kg^{-1}.

Recently, several groups reported another type of supercapacitor, so called active electrolyte enhanced supercapacitor (AEESC). In AEESCs the redox active species, which provide large pseudocapacitance, are dissolved in electrolyte rather than coated on the electrodes. For example, Roldán *et al.* added hydroquinone (HQ) in the H_2SO_4 electrolyte of supercapacitors with activated carbon or carbon nanotube as electrodes.[11] The specific capacitance of the electrode was increased from ~320 F g^{-1} in H_2SO_4 to 901 F g^{-1} in HQ/H_2SO_4 redox active electrolyte. During the charging process HQ was oxidized into *p*-benzoquinone (BQ) near positive electrode,[12] and when the device was discharged BQ was reduced back to HQ. Similarly, ferricyanide ($Fe(CN)_6^{4-}$), iodide (I^-), methylene blue and *p*-phenylenediamine were also employed as redox active electrolytes, significantly enhancing the performance of the supercapacitors.[13–17] Compared with solid redox active materials, active electrolytes are much easier to process, and compatible with the present fabrication technology of commercial supercapacitors. Therefore, AEESC is considered as a promising type of supercapacitor.

However, the previous investigations mainly focused on how to improve the specific capacitance by inducing active electrolyte, but neglected the effects of active electrolyte on the

self-discharging (SDC) process of the supercapacitors.[18] The rate of SDC is the index of the energy retention of a power storage device, and supercapacitors with high SDC rate are of little practical use due to the quick loss of stored energy. Unfortunately, most researchers did not report the SDC rate of their AEESCs, and from the limited examples it was found that the SDC of AEESC was faster compared with that of EDLSC.[18] If high SDC rate is the intrinsic property of AEESC, neglecting it will lead to overrating the practicability of AEESC. Although SDC process of EDLSC has been investigated both in theory and experiment,[19,20] the conclusions of these investigations help us little to understand the SDC of AEESC, because the working mechanism of the two types of supercapacitor are distinct. Therefore, in order to fully evaluate the performance of AEESCs, it is necessary to conduct a comprehensive research on their SDC process. In this paper, by taking HQ enhanced supercapacitor as example, we systematically investigated the SDC process of AEESC. It was found that the AEESC with HQ/H_2SO_4 as electrolyte showed a much faster SDC process compared with the EDLSC with pure H_2SO_4 as electrolyte. The electrode process on individual electrode of AEESC was analyzed and the mechanism of the SDC process was investigated quantitatively. The migration of the active electrolyte between two electrodes was believed to cause the SDC of AEESC. In order to inhabit the migration of active electrolyte, two different strategies were designed: using ion-exchange membrane as the separator, or choosing a special active electrolyte which is reversibly convertible to insoluble species during charge/discharge cycles. Following the above strategies, Nafion® membrane was tested as the separator in the AEESC containing HQ, and a novel AEESC with $CuSO_4$ as active electrolyte was fabricated. It was found that both devices showed improved specific capacitance compared with corresponding EDLSC, and much slower SDC process than conventional AEESCs.

Experimental

Materials

Natural graphite powders were bought from Qingdao Huatai lubricant sealing S&T Co.Ltd. Graphene oxide (GO) was prepared with modified Hummers method according to the literatures.[21,22] H_2SO_4 (98%), hydrazine momohydrate (80%), hydroquinone (AR) and copper sulfate (AR) were purchased from Sinopharm Chemical Reagent Co., Ltd. Nafion® 117 membrane was the product of DuPont.

Preparation of Graphene hydrogel

Graphene hydrogel (GHG) was prepared by reducing GO hydrothermally and followed by treating with hydrazine.[23,24] Briefly, 10 mL GO aqueous dispersion (2 mg mL^{-1}) was sealed in a Teflon-lined autoclave and maintained at 180 °C for 12 h. After the autoclave was cooled to room temperature, the black GHG block in the autoclave was taken out, immersed into an aqueous solution of hydrazine monohydrate (50 %), and treated at 95 ˚C for 8 h. Finally, the resulting GHG was purified by dialysis overnight in ultrapure water.

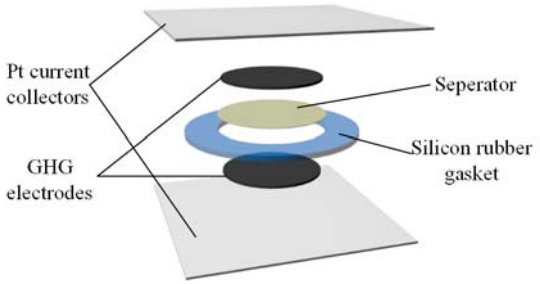

Fig. 1 Structure of the supercapacitors in this paper.

Fabrication of the Supercapacitors

The structure of the supercapacitor devices is illustrated in Fig. 1. Platinum foil was used as current collector, and a silicon rubber gasket with thickness of 1 mm and inner diameter of 12 mm was used to seal the device. GHG was employed as electrodes. The as-prepared GHG was immersed into the electrolyte overnight to exchange their interior water with electrolyte, and cut into small cylindrical pieces (with thickness of ~ 1 cm and diameter of ~ 0.8 cm). The GHG cylinders were compressed into thick discs under 600 kPa. Two of these GHG discs, together with platinum foils and a piece of separator were assembled into a layered structure, as shown in Fig. 1, and sandwiched between two glass slides which were hold together by a clamp. Four types of devices were fabricated, whose electrolytes are 1 M H_2SO_4 (Device 1), 0.4 M HQ + 1 M H_2SO_4 (Device 2 and Device 3), 0.4 M $CuSO_4$ + 1 M H_2SO_4 (Device 4), respectively. For Device 3, the separator was Nafion® 117 membrane, while for other three devices the separators were porous cellulose acetate membranes (pore size: 0.2 μm).

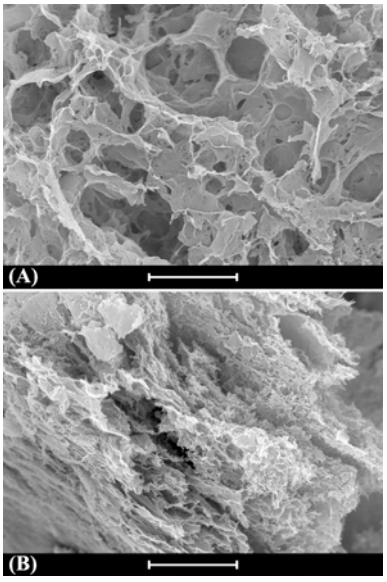

Fig. 2 SEM images of the GHG. (A) As-prepared GHG; (B) Compressed GHG electrode. Scale bar: 20 μm.

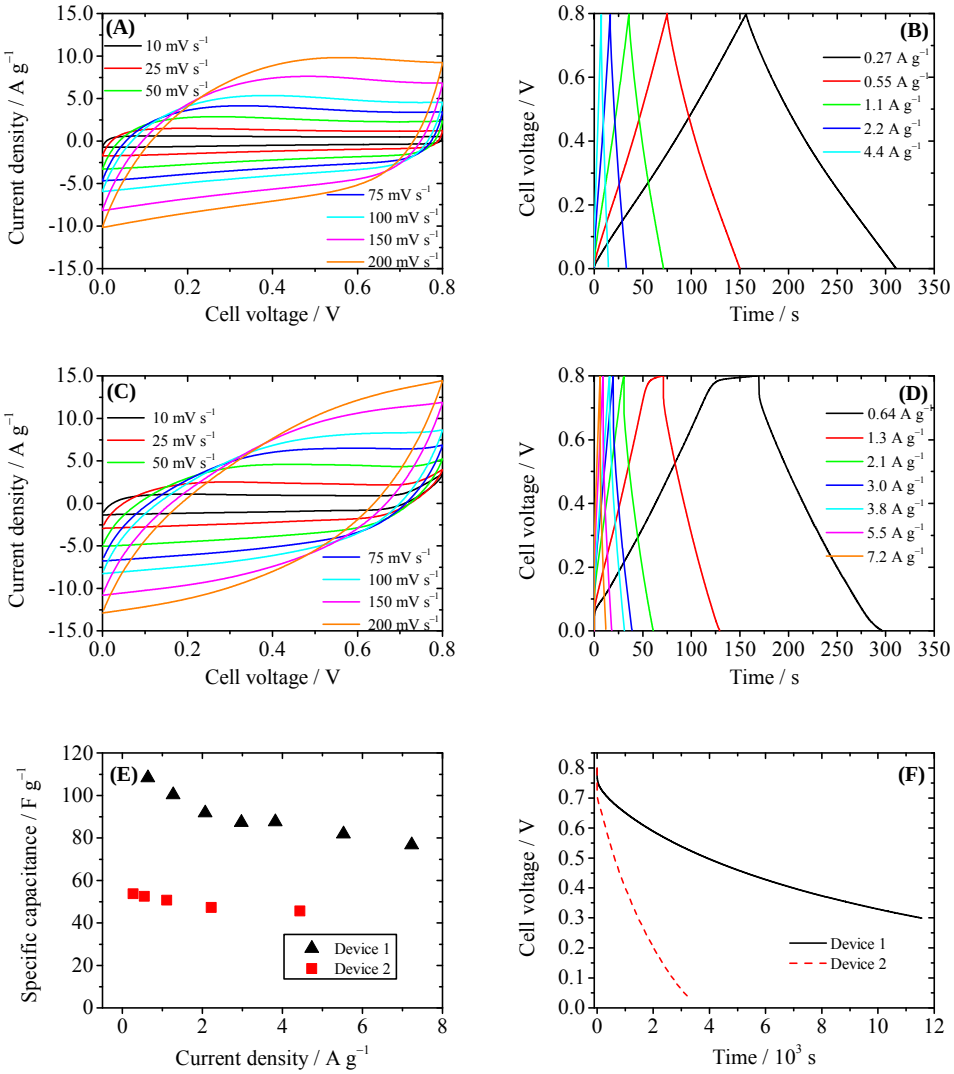

Fig. 3 Performance of Device 1 (1 M H_2SO_4 as electrolyte) and Device 2 (0.4 M HQ + 1 M H_2SO_4 as electrolyte). (A) Cyclic voltammograms of Device 1 at different scanning rate. (B) Galvanostatic charge-discharge curves of Device 1. (C) Cyclic voltammograms of Device 2 at different scanning rate. (D) Galvanostatic charge-discharge curves of Device 2. (E) Comparison of specific capacitances of Device 1 and Device 2. (F) SDC curves of Device 1 and 2, recorded after the devices were charged to 0.8 V at a constant current of 10 mA.

To conduct three-electrode measurements, the above device was immersed into an electrochemical cell filled with the same electrolyte as used in the device. Two channels were cut on the silicon rubber gasket, to ensure the connectivity of the electrolyte in the device and the cell. The two electrodes of the device were used as working and counter electrode, respectively, and a saturated calomel electrode (SCE) was used as reference electrode.

Characterization

The structure of GHG was characterized by Hitachi TM3000 scanning electronic microscope. All the electrochemical measurements were performed on a CHI 660D electrochemical workstation. Before test the device was activated by cyclic voltammetry cycling from 0 V to the work voltage of each device for 50 cycles.[25] The specific capacitance of the device was calculated from galvanostatic charge-discharge (GCD) curves according to the following equations:

$$C_s = \frac{Jt}{V - IR}, \quad (1)$$

$$J = \frac{I}{m}, \quad (2)$$

where J is the mass current density, I is the current applied on the device, t is the discharge time, m is the total mass of two electrodes, V is the highest voltage in the GCD curves, and IR represents the voltage drop at the beginning of the discharge process, caused by internal resistance of the device. The specific capacitance of single electrode was calculated from the GCD curves measured in three-electrode system:

$$C_+ \text{ or } C_- = \frac{Jt}{\Delta V - IR}, \quad (3)$$

$$J = \frac{I}{m}, \quad (4)$$

where m is the mass of single electrode, and ΔV is the potential change of the electrode during discharge process; I, t and IR have the same definitions as in Eqn. 1 and 2.

Results and discussion

In this paper graphene was chosen as the electrode material because it can provide high specific capacitance. Graphene electrodes in aqueous electrolyte were reported to have a specific capacitance of 160 F g^{-1} at high current density of 100 A g^{-1}.[23] And in organic electrolyte, KOH activated graphene material showed a high energy density of 70 Wh kg^{-1} and a very large power density of 2.5 × 10^5 W kg^{-1} at current 5.7 A g^{-1}, owing to the high working voltage (3.5 V).[26] Some of these performance is much higher than that of commercial carbon supercapacitors. The GHG used as electrode material was synthesized *via* self-assemble of chemically converted graphene (CCG) sheets during hydrothermal reduction of graphene oxide (GO).[27,28] As depicted in Fig 2A, the as-prepared GHG shows highly porous three-dimensional (3D) network composed of two-dimensional (2D) CCG sheets. The size of pores in GHG is in the range of several to tens of micrometers. During the assembly of supercapacitor device, GHG was compressed to ~15% of its original volume, and consequently the pore size decreased obviously, as shown in Fig. 2B. In spite of this, the pores in GHG electrode are still large enough for the diffusion of electrolyte.[29] The thickness of the GHG disc in the device was ~ 440 μm, and the mass density of the single electrode was 2.6 ~ 3.5 mg cm^{-2}.

To evaluate the performance of GHG electrode, a supercapacitor with 1 M H_2SO_4 as electrolyte (Device 1) was first fabricated and tested. As displayed in Fig. 3A, the CV curves of Device 1 are almost rectangular, with weak and wide redox waves around 0.4 V, which can be attributed to the redox of residual oxygen-containing functional groups on CCG sheets.[30] The GCD curves of Device 1 shown in Fig. 3B are nearly triangular, indicating that the capacitance of Device 1 is independent of cell voltage. The specific capacitances of Device 1 calculated from GCD curves are 50.8 F g^{-1} at 1.1 A g^{-1}, and 45.5 F g^{-1} at 4.4 A g^{-1}. These results are consistent with the literature data,[23,30] demonstrating that the prepared GHG is suitable electrode material for supercapacitors. We then investigated the GHG-based AEESC with HQ as active electrolyte (Device 2).[11] When HQ was added in the electrolyte, the electrochemical behavior of the device changed in several aspects. The shapes of CV curves of Device 2 (Fig. 3C) are still deformed rectangle, but the currents in CV curves of Device 2 are larger than those in Device 1, revealing that HQ provides additional capacitance. At high scan rate, the shapes of CV curves deviate from rectangle, becoming obviously tilted. This is caused by the larger capacitance and/or internal resistance of Device 2. At low scan rate, when the cell voltage of Device 2 rises above 0.7 V, the current increases sharply, and during the reverse scanning no cathodic current is observed. This phenomenon suggests that some irreversible electrochemical reactions take place at high cell voltage. In Fig. 3D, there exists a plateau at high cell voltage region of the charge curves with low current density (< 2.6 A g^{-1}), corresponding with the large current at the same voltage range in CV curves. Such a plateau is the characteristic of solvent decomposition.[31] In this voltage range, the current is consumed by the decomposition of water, thus the growth rate of cell voltage is very low. The specific capacitances of Device 2 calculated from GCD curves are 100.2 F g^{-1} at 1.3 A g^{-1}, and 76.8 F g^{-1} at 7.2 A g^{-1}, respectively. These values are nearly two times those of Device 1 (Fig. 3E), showing that the active electrolyte HQ significantly increases the specific capacitance of electrochemical capacitor.

However, when SDC of the capacitor device is taken into account, an obvious drawback of Device 2 arises. As depicted in Fig. 3F, the SDC process of Device 2 is much faster than that of Device 1. After 11524 s the cell voltage of Device 1 decreases to 0.3 V ($\tau_{0.3}$); however, $\tau_{0.3}$ of Device 2 is only 1462 s, and in 3100 s the cell voltage of Device 2 dwindles down from 0.8 V to 0.05 V. Noticing that the structure and package of both Device 1 and Device 2 are identical, their effects on the SDC process can be considered as system error, thus the comparison of the SDC time of the two devices distinctly reveals the fact that HQ strongly accelerates the SDC process. Fast SDC process will limit the practical application of the supercapacitor. Therefore, after the introduction of active electrolyte HQ, although the specific capacitance of the supercapacitor is improved, the practicability of the device becomes even worse.

To determine the mechanism of SDC process of the two devices, the SDC curves were analyzed with several established models. If the SDC of the capacitor is govern by current leakage over a resistance R (RC circuit), the cell voltage V can be described by

$$V = V_0 \exp\left(\frac{-t}{RC}\right), \quad (5)$$

where V_0 is the initial voltage of the cell. However, for both devices, the plot of ln$V$ against t did not gave straight line (See Fig. S1 in ESI†). In fact, since the packaging method of the two devices and the measurement system are identical, the leakage currents in the two devices are supposed to be similar, and cannot lead to such large difference in SDC rate. Thus the SDC process is not caused by current leakage over a resistance. Another well-accepted mechanism of SDC is the diffusion-control model. In this model the stored charges are lost due to the diffusion of the electrolyte ions in the EDL, and the cell voltage obeys following equation:[32]

$$V = V_0 - mt^{\frac{1}{2}}, \quad (6)$$

where *m* is the diffusion parameter and is decided by, for a given device, the initial voltage. Fitting of SDC curve of Device 1 shows that the cell voltage is proportional to the square root of time (R^2 = 0.999, as depicted in Fig. S2†), thus the SDC of Device 1 is probably controlled by diffusion of the ions in EDL.[19, 32] However, in Device 2, since the active electrolyte HQ and its oxidation product BQ are nearly electric neutral in H_2SO_4, and their diffusion coefficients are obviously smaller than those of H^+ and SO_4^{2+}, it is difficult to explain the fast SDC of Device 2 by diffusion of ions in EDL.

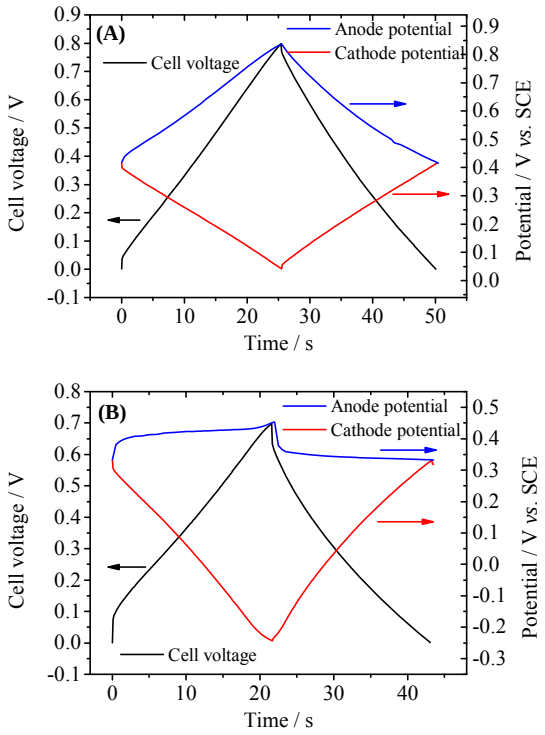

Fig. 4. Potential curves of single electrode of Device 1 (A) and Device 2 (B) during GCD. Current density: Device 1: anode, 3.2 A g^{-1} cathode：2.58 A g^{-1}; Device 2: anode, 4.8 A g^{-1}, cathode, 3.65 A g^{-1}.

In fact, the fast SDC process of Device 2 is closely related to the active electrolyte HQ, thus to explain the SDC process, the electrode processes on each individual electrode and mass transport in the device are taken into account. The potential change of single electrode in Device 1 and 2 are shown in Fig. 4. From Fig. 4A one can easily conclude that Device 1 is a symmetric capacitor, because during charge/discharge process the potential shift of each electrode is always half of the cell voltage. However, as represented in Fig. 4B, Device 2 is a typical asymmetric device. When current is applied on Device 2, a large IR drop appears in the potential curve of anode, but the potential of anode keeps almost unchanged for the rest charge process. When the cell voltage reaches 0.7 V, a tiny increase in anode potential of 0.06 V is observed, corresponding to a high specific capacitance of 1851.4 F g^{-1}. Since the total capacitance of the device is the series capacitance of two electrodes, the large specific capacitance of anode can significantly increase the total capacitance of the device. Meanwhile, the potential of cathode changes obviously during the charge process, from 0.33 V to a very negative potential of −0.24 V *vs.* SCE (Fig. 4B). At this negative potential, water is decomposed to release hydrogen. This can explain the appearance of solvent decomposition plateau on GCD curve of Device 2. The asymmetric specific capacitances of electrodes in Device 2 also suggest that an asymmetric device structure, with small anode mass and large cathode mass, can further enhance the specific capacitance of the device, by balancing the capacitances of two electrodes. The potential curves in Fig. 4B agree well with the results obtained in other HQ enhance supercapacitors with activated carbon as electrodes,[12] and can be explained by the redox reaction of HQ on anode. In fact, during charge/discharge process, following electrochemical reaction takes place on the surface of anode:

$$HQ \rightarrow BQ + 2\,H^+ + 2\,e^-$$

Thus the electrode reaction on the anode is a galvanostatic electrolysis. It has been confirmed by the previous investigation that this electrochemical reaction is reversible on graphene electrode.[33] Therefore, the electrode potential of anode during the galvanostatic electrolysis will change little as long as the electrolysis time is shorter than transition time.[34] Namely, HQ becomes an ideal depolarizer in the device, which pins the anode potential near its equilibrium electrode potential. According to the definition of capacitance (Eqn. 3), the capacitance of anode becomes ultralarge due to small potential change. Therefore, Faradaic process at anode is the origin of the large capacitance of Device 2.

As mentioned above, BQ is generated during charge process as the product of galvanostatic electrolysis of HQ, and dissolves in the electrolyte inside the channels of porous GHG anode. These BQ molecules will diffuse across the separator and reach the surface of cathode, as shown in Fig. 5. Since the potential of cathode drops to −0.24 *vs.* SCE *via* charging the EDL, BQ will be easily reduced by cathode. The reduction of BQ on the charged cathode is a coulostatic electrolysis in thin layer of solution. Noticing that the potential of cathode is much lower than the equilibrium potential of BQ/HQ, the electrochemical reaction is controlled by diffusion of BQ. For simplicity, it is assumed that at the beginning of SDC the initial concentration of BQ in the anode chamber and separator is uniform, and the diffusion coefficient of BQ in the porous separator and GHG electrode is identical, thus the total charge passing from cathode to the solution follows Eqn. 7[35]:

$$Q(t) = nFAVc_{BQ}\left\{1 - \frac{8}{\pi^2}\sum_{m=1}^{\infty}\left(\frac{1}{2m-1}\right)^2 \exp\left[\frac{-(2m-1)^2\pi^2 Dt}{l^2}\right]\right\} \quad (7)$$

where *A* is the area of the electrode, c_{BQ} is the initial concentration of BQ in the anode chamber, *V* is the volume of BQ solution, *n* is the number of electrons transferred in the reaction (n =2 for the reduction of BQ), *F* is the Faraday constant, *D* is the diffusion coefficient of BQ and *l* is the total thickness of the separator and anode. Since that the potential of cathode $V_-(t)$ can be expressed as

$$V_{-}(t) = V_{-}(0) + \frac{Q(t)}{C_{-}}, \quad (8)$$

and terms in Eqn. 6 for which m > 1 are negligibly small, the potential of cathode can be described by Eqn. 8:

$$V_{-}(t) = V_{-}(0) + \frac{nFAVc_{BQ}}{C} - \frac{8nFAVc_{BQ}}{\pi^2 C}\exp\left(\frac{-\pi^2 Dt}{l^2}\right). \quad (9)$$

Noticing that during the charge and discharge process the potential of anode V_+ keeps almost unchanged, we have

$$V(t) = V_{+} - V_{-}(t), \quad (10)$$

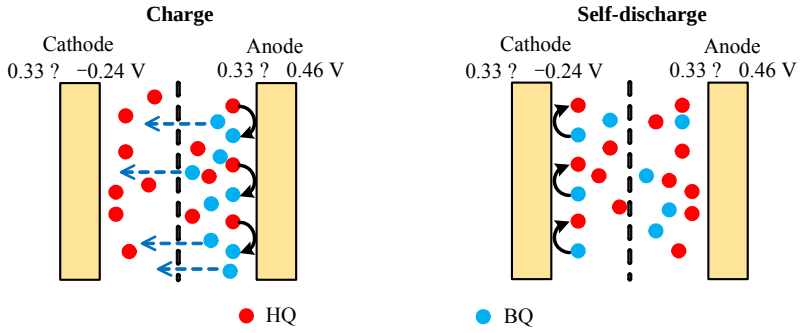

Fig. 5. Schematic sketch of mechanism of charge and SDC of AEESC.

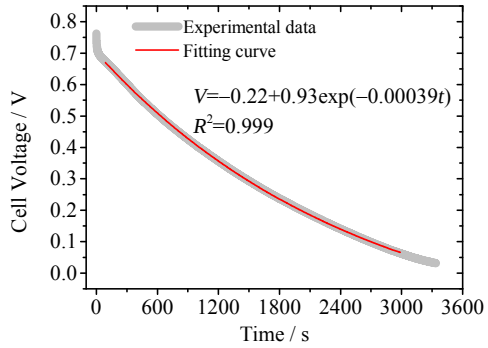

Fig. 6 Fitting results of the SDC curve of Device 2 to Eqn. 12.

and

$$V_{-}(0) = V_{+} - V(0). \quad (11)$$

By substituting Eqn. 9 and Eqn. 11 to Eqn. 10 it is obtained that

$$V(t) = V(0) - \frac{nFAVc_{BQ}}{C} + \frac{8nFAVc_{BQ}}{\pi^2 C}\exp\left(\frac{-\pi^2 Dt}{l^2}\right). \quad (12)$$

Eqn. 12 reveals that the cell voltage $V(t)$ decrease exponentially. It can be seen in Fig. 6 that the SDC curve fits well with Eqn. 12, giving a correlation coefficient of 0.999. It also suggests that the diffusion coefficient D and the thickness of the device strongly influence the SDC. From the fitting result the diffusion coefficient of BQ is calculated to be 1.2×10^{-7} cm^2 s^{-1}, smaller than the reported diffusion coefficient of BQ in H_2SO_4 (1.08×10^{-5} cm^2 s^{-1})[36], due to the fact that porous structure of GHG electrode and separator significantly increases the diffusion length.

At the initial stage of the SDC curve, there is a quick drop of cell voltage, resulting in deviation from the fitting result. This is probably caused by the decomposition of solvent. As mentioned above, solvent water will be reduced on cathode when the device is fully charged, and when the charge current is cut off this reduction process will go on, leading to a rapid increase in cathode potential. Such a process is not controlled by diffusion, and strongly depends on the surface property of the electrode (the overpotential of hydrogen evolution reaction). The platinum current collector in Device 2 may catalyze the hydrogen evolution reaction, but the fundamental reason is that the active electrolyte HQ shifts the working potential range of cathode beyond the electrochemical window of solvent, accelerating the SDC process.

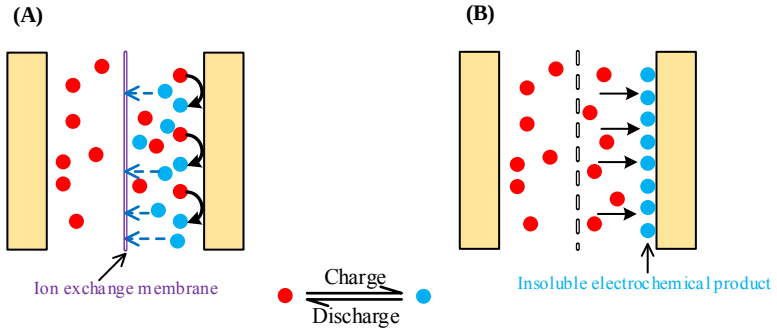

Fig. 7. Two strategies for inhibiting the migration of active electrolyte between two electrodes. (A) Using ion-exchange membrane as the separator; (B) choosing a special active electrolyte which is converted to insoluble species during charge process.

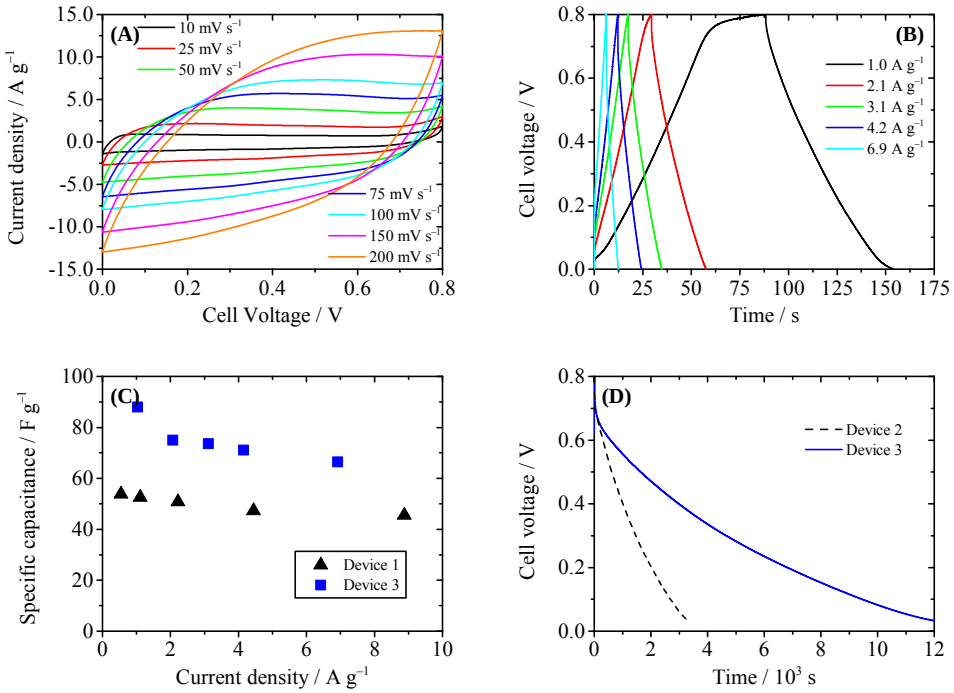

Fig. 8 Performance of Device 3 (with 0.4 M HQ + 1 M H_2SO_4 as electrolyte and Nafion® 117 as separator). (A) Cyclic voltammograms at different scanning rate. (B) Galvanostatic charge–discharge curves. (C) Caparation of specific capacitance of Device 1 and Device 3. (D) SDC curves of Device 2 and 3, recorded after the devices were charged to 0.8 V at a constant current of 10 mA.

According to above discussions, to suppress the fast SDC process of AEESCs, the first essential is to stop the shuttle of active electrolyte between two electrodes. To do so, we devised two strategies, as shown in Fig. 7: (1) using an ion-exchange membrane as the separator of the capacitor, which can block the migration of active electrolyte (Fig. 7A); (2) using a special active electrolyte which is converted to insoluble species and deposited onto the electrode during the electrochemical reaction in charge process, (Fig. 7B).

We first tried to improve HQ enhance supercapacitor following the first strategy. The porous separator in Device 2 was replaced by Nafion® 117 membrane (Device 3), which only allowed migration of H^+ ion across itself, thus the shuttle of BQ was inhibited. As displayed in Fig. 8A, the shapes of CV and GCD curves of Device 3 resemble those of Device 2, suggesting that the electrode processes are not changed by Nafion® film. The specific capacitances of Device 3 are calculated to be 75.0 F g^{-1} at 2.1 A g^{-1} and 66.4 F g^{-1} at 6.9 A g^{-1}, lower than those of Device 2, but still much higher than those of EDLSC Device 1 (Fig. 8C). Fig. 8D compares the SDC curves of Device 2 and 3. It can be observed in this figure that SDC process of Device 3 is much slower than that of Device 2. The cell voltage of Device 3 decreases from 0.8 V to 0.3 V after 4686 s, three times that of Device 2 (1462 s). This result reveals that Nafion® separator can successfully block the migration of active electrolyte and suppress the SDC process. However, the attenuation of cell voltage of Device 3 is still faster than Device 1. Thus, there exist some other minor paths of SDC in Device 3. One possible way is the decomposition of water, which also occurs in Device 2. This process can result in

sharp cell voltage decrease at the beginning of the SDC. Besides, HQ is reactive and can be converted into BQ by oxygen in air, thus a certain amount of BQ may be induced into the electrolyte as the impurity. Some of the BQ molecules in cathode chamber may survive after charge process, and they can also cause SDC by consuming the negative charges on cathode.

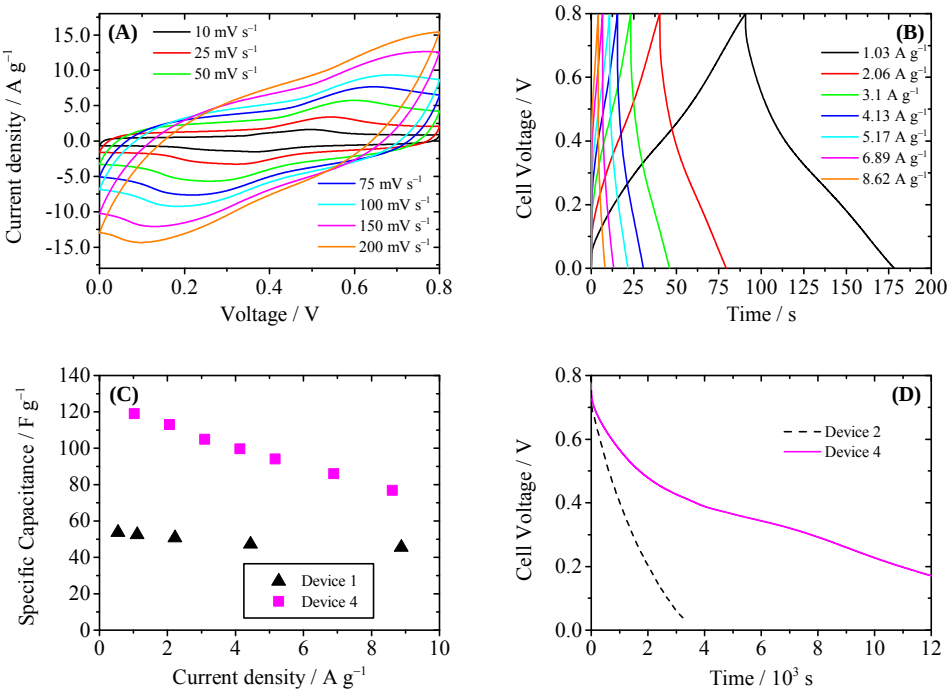

Fig. 9 Performance of Device 4 (with 0.4 M $CuSO_4$ + 1 M H_2SO_4 as electrolyte). (A) Cyclic voltammograms at different scanning rate. (B) Galvanostatic charge–discharge curves. (C) Comparison of specific capacitance of Device 1 and Device 4. (D) SDC curves of Device 2 and 4, recorded after the devices were charged to 0.8 V at a constant current of 10 mA.

To overcome the shortages of above devices, we designed another AEESC following strategy 2, by taking $CuSO_4$ as the active electrolyte (Device 4). In sulfonic acid, a following electrode reaction will occur, whose standard electrode potential is 0.34 V *vs.* SHE (standard hydrogen electrode):[37]

$Cu^{2+} + 2e^- = Cu$.

Thus when Device 4 is charged, Cu^{2+} ions are reduced to Cu metal (copper electroplate), which is insoluble in water and deposited onto the cathode. As a result, in Device 4 there will be no shuttle effect of the electrochemical product. The characterizations of the Device 4 are summarized in Fig. 9. In the CV curves of Device 4 (Fig. 9A), a pair of redox wave around 0.4 V is observed. This redox wave is different from those of Device 1, thus may be assigned to the redox reaction of CCG involving copper species. Fig. 9B is the GCD curves of Device 4. The GCD curves obviously deviate from ideal triangular, due to the above-mentioned electrochemical reaction. The specific capacitances of Device 4 calculated from GCD curves are 113 F g^{-1} at 2.1 A g^{-1}, and 86 F g^{-1} at 6.9 A g^{-1}, as shown in Fig. 9C. Similar as Device 2, the enhancement of specific capacitance of Device 4 comes from the Faradaic pseudocapacitance induced by electroactive Cu^{2+}. However, since the shuffle effect is suppressed, Device 4 shows much slower SDC process compared with Device 2. As depicted in Fig. 9D, it takes 7727 s that the cell voltage of Device 4 decreases from 0.8 V to 0.3 V through SDC, and this time is significantly longer than those of Device 2 (1462 s) and Device 3 (4686 s). From the SDC curve of Device 4 it is also found that there exists a plateau region around 0.35 V, which is consistent with the plateau in GCD curve.

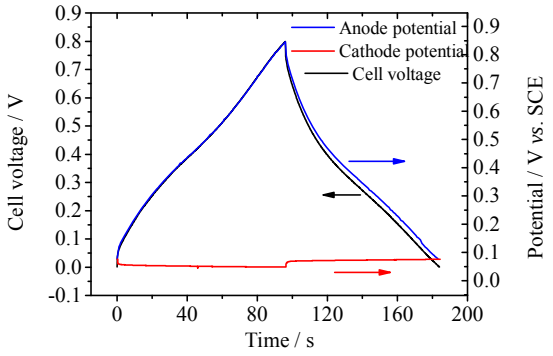

Fig. 10. Potential curves of single electrode of Device 4 during GCD at current density of 2.0 A g^{-1} (for anode) and 2.1 A g^{-1} (for cathode).

Also the electrode processes in Device 4 were investigated in three-electrode system. As shown in Fig. 10, during charge/discharge process, the potential shift of anode (0.77 V)

makes chief contribution to the increase of cell voltage, while the potential of cathode keeps stable (potential change: 0.03 V). The specific capacitance of cathode is calculated to be 14072.5 F g^{-1} at 2.1 A g^{-1}, and that of anode is 243.3 F g^{-1} at 2.0 A g^{-1}. As discussed above, the ultrahigh specific capacitance of cathode is the result of electrochemical reaction of Cu^{2+}. The Cu deposited on GHG electrode during charge process can be observed by SEM (Fig. S7†). The equilibrium potential of Cu^{2+}/Cu under experimental condition (0.4 M Cu^{2+} in 1 M H_2SO_4) is ~0.07 V *vs.* SCE or 0.252 V *vs.* SHE. As a result, the working potential range of anode is 0.252 ~ 1.052 V *vs.* SHE. Under this potential range the solvent water is stable (Noticing that the standard electrode potential of the reaction $O_2 + 4\ H^+ + 4\ e^- = 2\ H_2O$ is 1.229 V *vs.* SHE[37]). Therefore, SDC through decomposition of solvent, which occurs in Device 2 and 3, is avoided. Moreover, as described above, in Device 3 the oxidation product of BQ may be induced into the electrolyte and cause SDC. But in Device 4 the reduction product copper is not probably induced into electrolyte. Therefore, the charges stored on the electrode of Device 4 will not be lost through those additional redox processes. To conclude, with $CuSO_4$ as the active electrolyte, the capacitance of the supercapacitor is improved significantly, while the fast SDC process usually occurring in other AEESCs is suppressed.

Conclusions

In summary, in this paper, we systematically investigated the SDC processes of AEESCs. After incorporation of soluble electroactive species into supercapacitor device, although the capacitance of the device was increased, the SDC process was accelerated significantly. The migration of active electrolyte between two electrodes of the device (shuttle effect) is the primary reason for the fast SDC, as indicated by the analysis of electrode process of single electrode. In order to block the migration of active electrolyte between two electrodes, we developed two basic strategies: (1) using an ion-exchange membrane as the separator of the capacitor and (2) choosing a special active electrolyte which is converted to insoluble species during the electrochemical reaction in charge process. Two AEESCs were fabricated following these designs. It was confirmed that with Nafion® 117 membrane as separator, or with $CuSO_4$ as active electrolyte, the SDC of AEESC can be successfully suppressed. We believe that the results in this paper can guide the further design of AEESCs with both high energy density and good energy retention, and push forwards the development of supercapacitor in practical applications.

Acknowledgements

This work was supported by National Natural Science Foundation of China (21104041).

Notes and references

College of Materials, Xiamen University, Xiamen, 361005, P. R. China. E-mail: baihua@xmu.edu.cn; lilei@xmu.edu.cn

† Electronic Supplementary Information (ESI) available: Fitting results of SDC curves; AC impedance spectra and cycling stability of Device 3 and 4; SEM image and EDX of Cu coated GHG electrode. See DOI: 10.1039/b000000x/

1. P. Simon and Y. Gogotsi, *Nat. Mater.*, 2008, **7**, 845−854.
2. L. L. Zhang and X. S. Zhao, *Chem. Soc. Rev.*, 2009, **38**, 2520−2531.
3. G. Wang, L. Zhang and J. Zhang, *Chem. Soc. Rev.*, 2012, **41**. 797−828.
4. M. S. Whittingham, *Proc. IEEE*, 2012, **100**, 1518−1534.
5. W. T. Deng, X. B. Ji, Q. Y. Chen and C. E. Banks, *RSC Adv.*, 2011, **1**, 1171−1178.
6. C. D. Lokhande, D. P. Dubal and O. S. Joo, *Curr. Appl. Phys.*, 2011, **11**, 255−270.
7. G. A. Snook, P. Kao and A. S. Best, *J. Power Sources*, 2011, **196**, 1−12.
8. X. Zhao, B. M. Sanchez, P. J. Dobson and P. S. Grant, *Nanoscale*, 2011, **3**, 839−855.
9. H. Wang, H. S. Casalongue, Y. Liang and H. Dai, *J. Am. Chem. Soc.*, 2010, **132**, 7472−7477.
10. Y. F. Wang, X. W. Yang, L. Qiu and D. Li, *Energy Environ. Sci.*, 2013, **6**, 477−481.
11. S. Roldán, C. Blanco, M. Granda, R. Menéndez and R. Santamaría, *Angew. Chem. Int. Ed.*, 2011, **50**, 1699−1701.
12. S. Roldán, M. Granda, R. Menéndez, R. Santamaría and C. Blanco, *J. Phys. Chem. C*, 2011, **115**, 17606−17611.
13. S. Roldán, M. Granda, R. Menéndez, R. Santamaría and C. Blanco, *Electrochim. Acta*, 2012, **83**, 241−246.
14. J. Cong, X. Yang, L. Kloo and L. Sun, *Energy Environ. Sci.*, 2012, **5**, 9180−9194.
15. W. Chen, R. B. Rakhi and H. N. Alshareef, *Nanoscale.*, 2013, **5**, 4134−4138.
16. H. Yu, L. Fan, J. Wu, Y. Lin, M. Huang, J. Lin and Z. Lan, *RSC Adv.*, 2012, **2**, 6736−6740.
17. H. Yu, J. Wu, L. Fan, Y. Lin, S. Chen, Y. Chen, J. Wang, M. Huang, J. Lin, Z. Lan and Y. Huang, *Sci. Chin. Chem.*, 2012, **55**, 1319−1324.
18. M. Tachibana, T. Ohishi, Y. Tsukada, A. Kitajima, H. Yamagishi and M. Murakami, *Electrochemistry*, 2011, **79**, 882−886.
19. Q. Zhang, J. Rong, D. Ma and B. Wei, *Energy Environ. Sci.*, 2011, **4**, 2152−2159.
20. T. Tevi, H. Yaghoubi, J. Wang and A. Takshi, *J. Power Sources*, 2013, **241**, 589−596.
21. W. S. Hummers and R. E. Offeman, *J. Am. Chem. Soc.*, 1958, **80**, 1339−1339.
22. K. W. Chen, L. B. Chen, Y. Q. Chen, H. Bai and L. Li, *J. Mater. Chem.*, 2012, **22**, 20968−20976.
23. L. Zhang and G. Q. Shi, *J. Phys. Chem. C*, 2011, **115**, 17206−17212.
24. Y. X. Xu, Q. Wu, Y. Q. Sun, H. Bai and G. Q. Shi, *ACS Nano*, 2010, **4**, 7358−7362.
25. M. D. Stoller and R. S. Ruoff, *Energy Environ. Sci.*, 2010, **3**, 1294−1301.
26. Y. Zhu, S. Murali, M. D. Stoller, K. J. Ganesh, W. Cai, P. J. Ferreira, A. Pirkle, R. M. Wallace, K. A. Cychosz, M. Thommes, D. Su, E. A. Stach and R. S. Ruoff, *Science*, 2011, **332**, 1537−1541.
27. Y. X. Xu, K. X. Sheng, C. Li and G. Q. Shi, *ACS Nano*, 2010, **4**, 4324−4330.

28. C. Li and G. Shi, *Nanoscale*, 2012, **4**, 5549−5563.
29. H. Zhang, G. Cao, Y. Yang and Z. Gu, *Carbon*, 2008, **46**, 30−34.
30. K. X. Sheng, Y. X. Xu, C. Li and G. Q. Shi, *New Carbon Mater.*, 2011, **26**, 9−15.
31. S. Ban, J. Zhang, L. Zhang, K. Tsay, D. Song and X. Zou, *Electrochim. Acta*, 2013, **90**, 542−549.
32. B. W. Ricketts and C. Ton-That, *J. Power Sources*, 2000, **89**, 64−69.
33. C. L. He, C. L. Liu, T. P. Xie, Y. Wang, J. Zhang and L. Zhang, *Chem. J. Chin. Univ.-Chin.*, 2012, **33**, 1290−1294.
34. A. J. Bard and L. R. Faulkner, *Electrochemical Methods Fundamentals and Applications*, 2nd Edn., John Wiley & Sons., 2001.
35. A. T. Hubbard and D. G. Peters, *CRC Crit. Rev. Anal. Chem.*, 1973, **3**, 201−242.
36. X. S. Zhang, P. Ding, Y. C. Dai and W. K. Yuan, *Prog. Nat. Sci.*, 1999, **9**, 796−800.
37. W. M. Haynes and D. R. Lide, *Handbook of Chemistry and Physics*, 90 Edn., CRC Press, Boca Raton, 2010.